Quasibound states of tetrahedral quantum structures

A. D. Barr, F. J. Estrella, and L. E. Reichl*
Center for Complex Quantum Systems and Department of Physics, The University of Texas at Austin, Austin, Texas 78712, USA

(Received 20 December 2019; accepted 23 January 2020; published 18 February 2020)

Chemical reaction dynamics is known to be influenced by quasibound states (unstable electron standing waves) that exist in the positive-energy continuum in the spatial neighborhood of molecules. These unstable spatial structures give rise to resonances in the scattering dynamics between molecules or between electrons and molecules. Here we analyze the quasibound states associated with both an attractive and a repulsive molecule-size tetrahedral structure by using Wigner-Eisenbud *R*-matrix theory. Our results indicate that quasibound states typically exist in the neighborhood of all small molecules and other small quantum objects.

DOI: 10.1103/PhysRevA.101.022706

I. INTRODUCTION

The atomic structure of molecules largely determines the spatial distribution of electrons attached to the atoms that comprise the molecule. The electrons form bound-state (negative energy) quantum standing waves on the molecular structure, and they can also form quasibound (positive energy) standing waves that can exist in the positive-energy continuum. Although quasibound states have a finite lifetime, they can have a large influence on the dynamics of chemical reactions [1,2]. Visualization of the spatial structure of quasibound states has proved elusive. However, recent experiments have begun to image their spatial structure [3,4].

An important tool for determining the energy of quasibound states is scattering theory because quasibound states generally give rise to scattering resonances. However, numerical simulations of quantum waves scattering from a molecule, or other extended objects, can be daunting, because the analysis of the scattering process generally has to be repeated for each incident energy. In Ref. [5], a formalism was developed to study wave scattering from two- and three-dimensional localized objects using Wigner-Eisenbud (W-E) scattering theory [6,7] (also called *R*-matrix theory). This formalism forms the model for the approach we use here. Wigner-Eisenbud scattering theory has a long and distinguished history. It was first developed by Wigner and Eisenbud to study nuclear scattering processes [8] and subsequently as a framework to compare predictions of random matrix theory to experimental nuclear scattering data [9,10]. It has been used extensively to model atomic scattering processes [11–14] and electron-molecule collisions [15–18]. W-E scattering theory has also been used to study quasibound state formation in a two degree of freedom (DoF) model of HO-Cl dissociation [19,20], electron scattering in two DoF waveguides [21–23], scattering of waves from a chaotic system with cylindrical symmetry [24–26], scattering from periodic lattices [27,28], and a search for bound states in the energy continuum [29]. In subsequent sections, we show that W-E scattering theory provides a means to visualize the structure of quasibound-electron waves that form in the positive-energy continuum of three DoF objects.

In addition to the study of quantum wave dynamics in molecules and small quantum devices, the study of electromagnetic waves in optical microcavities has become a field of growing interest [30]. For example, Nöckel, Stone, and Redding [31,32] showed that D-shaped optical resonators with internal chaotic dynamics [33] could be used to construct lasers with unique directional emissions. These new applications of small open quantum and electromagnetic systems invite a detailed examination of the quantum dynamics (wave properties) of other small quantum systems that could be used to model unique nanometer scale quantum and optical devices.

In subsequent sections, we explore the quantum wave dynamics of a molecule-size tetrahedron and use W-E theory to analyze the scattering properties of a complex three-dimensional object. Molecules with tetrahedral structure occur commonly in nature. Nuclei whose distribution of protons and neutrons have tetrahedral symmetry have high stability [34–36] and have been suggested as a means to explain the order of elements in the periodic table [37]. Tetrahedral structures have been shown to have fractal scattering properties [38]. Thus, the scattering of waves from tetrahedrons is relevant for molecules, atomic nuclei, and even metal clusters [39].

W-E theory decomposes configuration space into a reaction region that fully contains the potential-energy distribution and an asymptotic scattering region in which the potential energy is zero. The asymptotic region can be characterized by a complete set of good quantum numbers. The reaction region may be partially chaotic and does not have a complete set of good quantum numbers. However, it can be described in terms of a complete set of basis states that satisfy certain boundary conditions on the interface between the reaction and asymptotic regions. The reaction region basis states are then coupled to the asymptotic region through a singular coupling [40,41].

We begin in Sec. II with a description of the tetrahedron system. In Sec. III, we formulate the exact scattering problem

*reichl@mail.utexas.edu

for the three-dimensional system considered here. In Sec. IV, we formulate the W-E scattering theory. In Sec. V, we describe the scattering properties of the attractive tetrahedron and show the structure of some of its quasibound states. In Sec. VI, we perform a similar analysis for the repulsive tetrahedron. And finally in Sec. VII, we make some concluding remarks.

II. TETRAHEDRON SYSTEM

We consider a particle of mass m_1 (an atom or an electron for example) scattering from the tetrahedron which has mass m_2 and is extended in space but fairly localized (falls off faster than $\frac{1}{r}$). Let us assume that, in the laboratory frame, m_1 has displacement $\hat{\mathbf{r}}_1$ and m_2 has displacement $\hat{\mathbf{r}}_2$. The relative displacement of the two masses is $\hat{\mathbf{r}} = \hat{\mathbf{r}}_2 - \hat{\mathbf{r}}_1$ and their center-of-mass displacement is $\hat{\mathbf{R}} = \frac{m_1}{M}\hat{\mathbf{r}}_1 + \frac{m_2}{M}\hat{\mathbf{r}}_2$, where $M = m_1 + m_2$ is the total mass. We will assume that the interaction potential energy $V(\hat{\mathbf{r}})$ depends only on the relative displacement of the two objects. We let $\hat{\mathbf{p}}_1$ and $\hat{\mathbf{p}}_2$ denote the momentum of particles m_1 and m_2, respectively, in the laboratory frame. The center-of-mass momentum is $\hat{\mathbf{P}} = \hat{\mathbf{p}}_1 + \hat{\mathbf{p}}_2$ and the relative momentum is $\hat{\mathbf{p}} = \frac{m_1}{M}\hat{\mathbf{p}}_2 - \frac{m_2}{M}\hat{\mathbf{p}}_1$. The Hamiltonian for this system is

$$\hat{H} = \frac{\hat{p}_1^2}{2m_1} + \frac{\hat{p}_2^2}{2m_2} + V(\hat{\mathbf{r}}) = \frac{\hat{P}^2}{2M} + \frac{\hat{p}^2}{2\mu} + V(\hat{\mathbf{r}}), \quad (1)$$

where $\mu = \frac{m_1 m_2}{(m_1+m_2)}$ is the reduced mass. Because the Hamiltonian is independent of $\hat{\mathbf{R}}$, the center-of-mass momentum is a constant of the motion. We can assume that the center-of-mass momentum is zero and set $\hat{\mathbf{P}} = 0$ without loss of generality.

The total angular momentum of the system can be written as

$$\hat{\mathbf{L}} = \hat{\mathbf{r}}_1 \times \hat{\mathbf{p}}_1 + \hat{\mathbf{r}}_2 \times \hat{\mathbf{p}}_2 = \hat{\mathbf{R}} \times \hat{\mathbf{P}} + \hat{\mathbf{r}} \times \hat{\mathbf{p}}. \quad (2)$$

The center-of-mass angular momentum $\hat{\mathbf{L}}_{\rm cm} = \hat{\mathbf{R}} \times \hat{\mathbf{P}}$ is a constant of the motion and can be set to zero without loss of generality. For interaction potentials of the type $V = V(\hat{\mathbf{r}})$, the relative angular momentum of the particles can change during the scattering process.

The energy eigenstates $|\Psi_E\rangle$, which describe the scattering process, satisfy the time-independent Schrödinger equation $\hat{H}|\Psi_E\rangle = E|\Psi_E\rangle$. In spherical coordinates, (r, θ, ϕ), the time-independent Schrödinger equation can be written

$$\hat{H}\Psi_E(\mathbf{r}) = -\frac{\hbar^2}{2\mu}\left[\frac{1}{r^2}\frac{\partial}{\partial r}\left(r^2\frac{\partial}{\partial r}\right)\right]\Psi_E(\mathbf{r}) + \frac{\hat{L}^2}{2\mu r^2}\Psi_E(\mathbf{r}) + V(\mathbf{r})\Psi_E(\mathbf{r}) = E\Psi_E(\mathbf{r}), \quad (3)$$

where $\hbar$ is Planck's constant, μ is the reduced mass of the system, $\Psi_E(\mathbf{r})$ is the probability amplitude, and $\hat{L}^2$ is the angular-momentum operator

$$\hat{L}^2 = -\hbar^2\left[\frac{1}{\sin(\theta)}\frac{\partial}{\partial\theta}\left(\sin(\theta)\frac{\partial}{\partial\theta}\right) + \frac{1}{\sin^2(\theta)}\frac{\partial^2}{\partial\phi^2}\right]. \quad (4)$$

The eigenstates of $\hat{L}^2$ are the spherical harmonics $Y_\ell^m(\theta, \phi)$ so that

$$\hat{L}^2 Y_\ell^m(\theta, \phi) = \hbar^2\ell(\ell+1)Y_\ell^m(\theta, \phi). \quad (5)$$

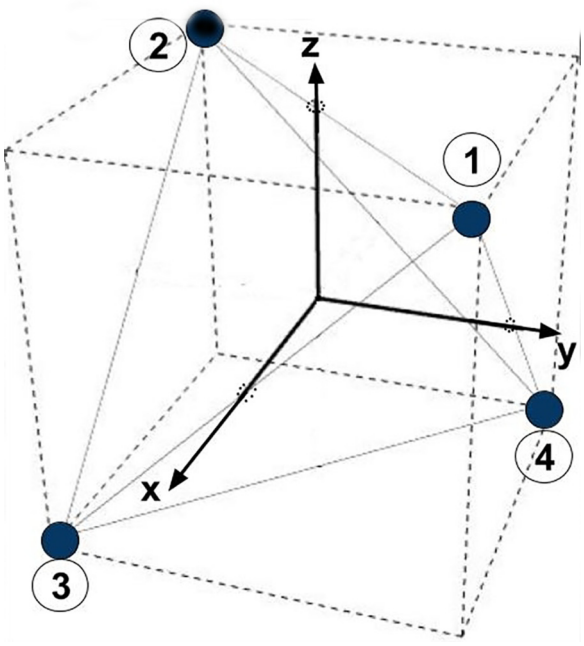

FIG. 1. Schematic picture of the tetrahedron.

We assume that the particle moves in a tetrahedral potential. The basic geometry of a tetrahedron is shown in Fig. 1. A potential with this basic structure can be modeled by the following function:

$$V(r,\theta,\phi) = U_0\left(\frac{1}{\sqrt{2\pi}\sigma}\right)^2\frac{1}{3\alpha}e^{-\frac{(r-r_0)^2}{2\sigma^2}}e^{-\frac{(\theta-0.9553)^2}{2\sigma^2}}\vartheta_3 \times\left(\frac{\pi(\phi-3\pi/4)}{3\alpha}, e^{-\frac{\epsilon^2\pi^2}{2\alpha^2}}\right) + U_0\left(\frac{1}{\sqrt{2\pi}\sigma}\right)^2\frac{1}{3\alpha}e^{-\frac{(r-r_0)^2}{2\sigma^2}}e^{-\frac{(\theta-(\pi-0.9553))^2}{2\sigma^2}}\vartheta_3 \times\left(\frac{\pi(\phi-5\pi/4)}{3\alpha}, e^{-\frac{\epsilon^2\pi^2}{2\alpha^2}}\right), \quad (6)$$

where θ_3 is an elliptic theta function, r_0 is the radius of the sphere that the four corners of the tetrahedron sit on, $\alpha = 1.0$ determines the number of potential wells along the ϕ direction, $\epsilon = 0.25$, and $\sigma = 0.25$ determines the standard deviation of the widths of the potential wells. In Fig. 2, we

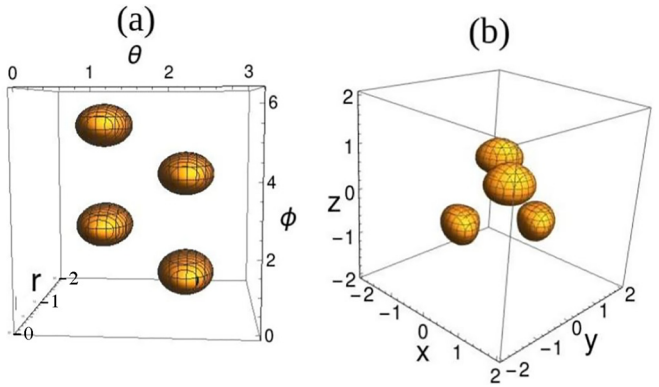

FIG. 2. The tetrahedron formed from elliptic theta functions: (a) spherical coordinates, (b) Cartesian coordinates.

plot this potential energy for $r_0 = 1.0$ d.u. and $U_0 = 10$ d.u. (d.u. denotes dimensionless units).

Throughout, we use the following units, based roughly on those of tetrahedral molecules [42], and the quasibound state structures that we find should be fairly typical of those molecules: The spacing between atoms at the corners of the tetrahedron is about $d = 2.24$ Å, which means they lie on a sphere of radius $a = \sqrt{\frac{3}{8}}2.24$ Å $= 1.37$ Å. We take as our energy unit $E_0 = \frac{\hbar^2}{\mu a^2} = 5.9 \times 10^{-10}$ ergs $= 3.62$ eV. We consider both an attractive tetrahedral distribution of potential wells with $U_0 = -10E_0$, $r_0 = 1a$, and a repulsive distribution of potential peaks with $U_0 = +10E_0$, $r_0 = 1a$. Therefore, the depth or height of our potential is about 36 eV.

III. THE REACTION AND SCATTERING MATRICES

To solve the scattering problem, it is useful to divide the scattering system into a reaction region that fully contains the scattering potential, and an asymptotic region outside any influence from the scattering potential. The energy eigenfunction $\Psi_E(\mathbf{r}) = \langle \mathbf{r}|\Psi_E\rangle$ [the solution to Eq. (3)] is then divided into a part that lies in the reaction region ($r < a$), $\Psi_E^R(\mathbf{r})$, and a part that lies in the asymptotic region ($r > a$), $\Psi_E^A(\mathbf{r})$. The functions $\Psi_E^R(\mathbf{r})$ and $\Psi_E^A(\mathbf{r})$ and their slopes must be continuous across the $r = a$ interface. This can be accomplished by equating the logarithmic derivatives of these two functions at the interface so that

$$\frac{\dot{\Psi}_E^R(a,\theta,\phi)}{\Psi_E^R(a,\theta,\phi)} = \frac{\dot{\Psi}_E^A(a,\theta,\phi)}{\Psi_E^A(a,\theta,\phi)}, \tag{7}$$

where $\dot{\Psi}_E(a,\theta,\phi) \equiv \frac{\partial \Psi_E(r,\theta,\phi)}{\partial r}|_{r=a}$.

In the asymptotic region, angular momentum and energy are conserved because $V(\hat{\mathbf{r}}) = 0$. $\Psi_E^A(\mathbf{r})$ will be a superposition of incident and scattered waves. Thus, it can be written in the form

$$\Psi_E^A(\mathbf{r}) = \sum_{\ell=0}^{\infty}\sum_{m=-\ell}^{\ell}\left[A_{\ell,m}\chi_{\ell,m}^{\text{in}}(kr) + B_{\ell,m}\chi_{\ell,m}^{\text{out}}(kr)\right]Y_{\ell,m}(\theta,\phi), \tag{8}$$

where $\chi_{\ell,m}^{\text{in}}(kr)$ [$\chi_{\ell,m}^{\text{out}}(kr)$] contains the radial dependence of incoming (outgoing) waves with energy E and quantum numbers ℓ, m.

In the reaction region, the wave function takes the form

$$\Psi_E^R(\mathbf{r}) = \sum_{\ell=0}^{\infty}\sum_{m=-\ell}^{\ell}\phi_{E,\ell,m}(r)Y_{\ell,m}(\theta,\phi), \tag{9}$$

where the form of $\phi_{E,\ell,m}(r)$ depends on the interaction potential. Angular momentum will be conserved only if the interaction potential is spherically symmetric, $V = V(|\mathbf{r}|)$. When angular momentum is conserved, each value of (ℓ, m) in $\Psi_E^A(\mathbf{r})$ couples only to the same value of (ℓ, m) in $\Psi_E^R(\mathbf{r})$.

The R matrix $R_{\nu_1;\nu_2}$, where $\nu_1 = \{\ell_1, m_1\}$ and $\nu_2 = \{\ell_2, m_2\}$, relates the value of $\Psi_E^A(\mathbf{r})$ with angular-momentum channel $\{\ell_1, m_1\}$ to the slope of $\Psi_E^A(\mathbf{r})$ with angular-momentum channel $\{\ell_2, m_2\}$ at the interface. The R matrix thus satisfies

$$\sum_{\ell_2=0}^{\infty}\sum_{m_2=-\ell_2}^{\ell_2} aR_{\nu_1,\nu_2}(E)\left[A_{\nu_2}\dot{\chi}_{\nu_2}^{\text{in}}(ka) + B_{\nu_2}\dot{\chi}_{\nu_2}^{\text{out}}(ka)\right] = A_{\nu_1}\chi_{\nu_1}^{\text{in}}(ka) + B_{\nu_1}\chi_{\nu_1}^{\text{out}}(ka), \tag{10}$$

where $\chi_\nu^{\text{in}}(ka) = h_l^{(2)}(ka)$ and $\chi_\nu^{\text{out}}(ka) = h_l^{(1)}(ka)$ ($h_l^{(2)}$ and $h_l^{(1)}$ are spherical Hankel functions). The quantity $R_{\nu,\nu'}(E)$ is the (ν, ν')th element of the R matrix. More explicitly, Eq. (10) takes the form

$$\sum_{\ell',m'} aR_{\ell,m;\ell',m'}(E)\dot{h}_{\ell'}^{(2)}(ka)A_{\ell',m'} + \sum_{\ell',m'} aR_{\ell,m;\ell',m'}(E)\dot{h}_{\ell'}^{(1)}(ka)B_{\ell',m'} = A_{\ell,m}h_\ell^{(2)}(ka) + B_{\ell,m}h_\ell^{(1)}(ka), \tag{11}$$

where $\dot{h}_{\ell'}^{(2)}(ka) = \frac{\partial h_{\ell'}^{(2)}(kr)}{\partial r}|_{r=a}$.

The scattering matrix relates the coefficients $A_{\ell,m}$ of incoming states to coefficients $B_{\ell,m}$ of outgoing states. Equation (11) can be written in matrix form as

$$a\bar{\bar{R}}(E)\cdot\bar{\bar{h}}^{(2)}\cdot\bar{A} + a\bar{\bar{R}}(E)\cdot\bar{\bar{h}}^{(1)}\cdot\bar{B} = \bar{\bar{h}}^{(2)}\cdot\bar{A} + \bar{\bar{h}}^{(1)}\cdot\bar{B}, \tag{12}$$

where $\bar{\bar{R}}(E)$ is a $M \times M$ matrix, $\bar{A}$ and $\bar{B}$ are $M \times 1$ column matrices, and $\bar{\bar{h}}^{(2)}$ and $\bar{\bar{h}}^{(1)}$ are $M \times M$ diagonal matrices. The S matrix $\bar{\bar{S}}(E)$ is given by the relation $\bar{B} = \bar{\bar{S}}(E)\cdot\bar{A}$. Solving Eq. (12) for $\bar{B}$, we get

$$\bar{\bar{S}}(E) = -[\bar{\bar{h}}^{(1)} - a\bar{\bar{R}}\cdot\bar{\bar{h}}^{(1)}]^{-1}\cdot[\bar{\bar{h}}^{(2)} - a\bar{\bar{R}}\cdot\bar{\bar{h}}^{(2)}]. \tag{13}$$

To simplify the notation, let $\bar{\chi}_{\text{in}} = \bar{\bar{h}}^{(2)}$ and $\bar{\chi}_{\text{out}} = \bar{\bar{h}}^{(1)}$. Then

$$\bar{\bar{S}}(E) = -[\bar{\chi}_{\text{out}} - a\bar{\bar{R}}\cdot\bar{\dot{\chi}}_{\text{out}}]^{-1}\cdot[\bar{\chi}_{\text{in}} - a\bar{\bar{R}}\cdot\bar{\dot{\chi}}_{\text{in}}]. \tag{14}$$

The general structure of the R matrix and the S matrix is determined by the behavior of states in the reaction region. The R matrix is nondiagonal in the indices ν when angular momentum is not conserved in the reaction region. This means that incident waves with quantum numbers $\{E, \nu\}$ give rise to outgoing waves with quantum numbers $\{E, \nu'\}$. Conversely, when angular momentum is conserved in the reaction region, the R matrix is diagonal in indices ν.

IV. WIGNER-EISENBUD SCATTERING THEORY

The tetrahedral potential energy is spatially localized. This allows us to separate the system into a "reaction region" ($0 \leqslant r \leqslant a$,), which fully contains the tetrahedral potential, and an asymptotic region ($a \leqslant r \leqslant \infty$) in which the potential energy is effectively zero. This spatial separation can be accomplished by using projection operators. Let

$$\hat{Q} = \int_0^a r^2 dr \int_0^\pi \sin(\theta)d\theta \int_0^{2\pi} d\phi |r,\theta,\phi\rangle\langle r,\theta,\phi| \tag{15}$$

project onto the reaction region $0 \leqslant r \leqslant a$ and let

$$\hat{P} = \int_a^\infty r^2 dr \int_0^\pi \sin(\theta)d\theta \int_0^{2\pi} d\phi |r,\theta,\phi\rangle\langle r,\theta,\phi| \tag{16}$$

project onto the asymptotic region $a \leqslant r \leqslant \infty$, where the states $|r, \theta, \phi\rangle$ are delta normalized,

$$\langle r_1, \theta_1, \phi_1 | r_2, \theta_2, \phi_2 \rangle = \frac{1}{r_1^2 \sin(\theta_1)} \delta(r_2 - r_1)\delta(\theta_2 - \theta_1)\delta(\phi_2 - \phi_1). \quad (17)$$

It is straightforward to show that $\hat{P}\hat{P} = \hat{P}$, $\hat{Q}\hat{Q} = \hat{Q}$, and $\hat{P}\hat{Q} = 0$ so that $\hat{P} + \hat{Q} = \hat{1}$. Then the eigenvalue equation $\hat{H}|E\rangle = E|E\rangle$ takes the form

$$\hat{Q}\hat{H}\hat{Q}|E\rangle + \hat{Q}\hat{H}\hat{P}|E\rangle = E\hat{Q}|E\rangle, \quad (18)$$

$$\hat{P}\hat{H}\hat{P}|E\rangle + \hat{P}\hat{H}\hat{Q}|E\rangle = E\hat{P}|E\rangle. \quad (19)$$

We can write the projections of the Hamiltonian into the reaction and asymptotic regions.

$$\hat{Q}\hat{H}\hat{Q} = \oint_{\mathbf{R}} d\mathbf{r}|r, \theta, \phi\rangle \left\{ -\frac{\hbar^2}{2\mu}\left[\frac{1}{r^2}\frac{\partial}{\partial r}\left(r^2\frac{\partial}{\partial r}\right)\right] + \frac{\hat{L}^2}{2\mu r^2} + V(\mathbf{r})\right\}\langle r, \theta, \phi|, \quad (20)$$

and

$$\hat{P}\hat{H}\hat{P} = \oint_{\mathbf{A}} d\mathbf{r}|r, \theta, \phi\rangle \left\{ -\frac{\hbar^2}{2\mu}\left[\frac{1}{r^2}\frac{\partial}{\partial r}\left(r^2\frac{\partial}{\partial r}\right)\right] + \frac{\hat{L}^2}{2\mu r^2}\right\}\langle r, \theta, \phi|, \quad (21)$$

respectively, where

$$\oint_{\mathbf{R}} d\mathbf{r} = \int_0^a r^2 dr \int_0^\pi \sin(\theta) d\theta \int_0^{2\pi} d\phi \text{ and}$$
$$\oint_{\mathbf{A}} d\mathbf{r} = \int_a^\infty r^2 dr \int_0^\pi \sin(\theta) d\theta \int_0^{2\pi} d\phi. \quad (22)$$

The coupling terms $\hat{Q}\hat{H}\hat{P}$ and $\hat{P}\hat{H}\hat{Q}$ are defined in terms of the singular operator [40,41], which can be written as

$$\hat{\mathcal{V}} = -\frac{2\hbar^2}{\mu}\frac{1}{a^2}\delta(r - a)\frac{\partial}{\partial r}, \quad (23)$$

so that

$$\hat{Q}\hat{H}\hat{P} = -\hat{Q}\hat{\mathcal{V}}\hat{P} = \frac{2\hbar^2}{\mu a^2}\oint_{\mathbf{R}} d\mathbf{r}_1 \oint_{\mathbf{A}} d\mathbf{r}_2 |\mathbf{r}_1\rangle\langle\mathbf{r}_1|\mathbf{r}_2\rangle\delta(r_2 - a)\frac{\partial}{\partial r_2}\langle\mathbf{r}_2|, \quad (24)$$

where $|\mathbf{r}_1\rangle = |r_1, \theta_1, \phi_1\rangle$.

We next introduce eigenstates $\hat{Q}|\phi_\alpha\rangle$ of the reaction region Hamiltonian $\hat{Q}\hat{H}\hat{Q}$ and eigenstates, $\hat{P}|\Phi(\mathbf{k})\rangle$, of the asymptotic region Hamiltonian $\hat{P}\hat{H}\hat{P}$. Then, the exact energy eigenstates can be expanded in the form

$$|E\rangle = \sum_{\alpha=1}^{\infty} \gamma_\alpha(E)\hat{Q}|\phi_\alpha\rangle + \Gamma_{\mathbf{k}}(E)\hat{P}|\Phi(\mathbf{k})\rangle, \quad (25)$$

where $\gamma_\alpha(E) = \langle\phi_\alpha|E\rangle$ and $\Gamma_{\mathbf{k}}(E) = \langle\Phi(\mathbf{k})|E\rangle$ are complex coefficients that determine the weight of the contribution of each of the basis states $\hat{Q}|\phi_\alpha\rangle$ and $\hat{P}|\Phi(\mathbf{k})\rangle$, respectively, to the energy eigenstates $|E\rangle$ of the system.

A. Reaction region eigenstates

The eigenvalue problem in the reaction region can be written

$$\hat{H}_{QQ}\hat{Q}|\phi_\alpha\rangle = \lambda_\alpha\hat{Q}|\phi_\alpha\rangle, \quad (26)$$

where $H_{QQ} = \hat{Q}\hat{H}\hat{Q}$. The eigenstates $\hat{Q}|\phi_\alpha\rangle$ are orthonormal and complete so

$$\langle\phi_\alpha|\hat{Q}|\phi_{\alpha'}\rangle = \delta_{\alpha,\alpha'} \text{ and } \sum_\alpha \hat{Q}|\phi_\alpha\rangle\langle\phi_\alpha|\hat{Q} = \hat{Q}. \quad (27)$$

The reaction region eigenstates in the position basis can be written

$$\langle\mathbf{r}|\hat{Q}|\phi_\alpha\rangle = \sum_{\ell=0}^{\infty}\sum_{m=-\ell}^{\ell}\sum_{n=1}^{\infty} C^\alpha_{\ell,m,n}N_{\ell,n}j_\ell\left(\frac{\kappa_{\ell,n}}{a}r\right)Y_\ell^m(\theta, \phi), \quad (28)$$

where $\kappa_{\ell,n}$ ensures that the Bessel function $j_\ell(\frac{\kappa_{\ell,n}}{a}r)$ has zero slope at $r = a$ and $N_{\ell,m}$ is the normalization constant

$$N_{\ell,n} = \left[\int_0^a r^2 dr\, j_\ell^2\left(\frac{\kappa_{\ell,n}}{a}r\right)\right]^{-1/2}. \quad (29)$$

Note also the normalization condition

$$\int_0^\pi \sin(\theta)d\theta \int_0^{2\pi} d\phi Y^*_{\ell_1,m_1}(\theta, \phi)Y_{\ell_2,m_2}(\theta, \phi) = \delta_{\ell_1,\ell_2}\delta_{m_1,m_2}. \quad (30)$$

The eigenvalue equation in the reaction region takes the form

$$\langle\mathbf{r}|\hat{Q}\hat{H}\hat{Q}|\mathbf{r}\rangle\langle\mathbf{r}|\hat{Q}|\phi_\alpha\rangle = \left\{-\frac{\hbar^2}{2\mu}\left[\frac{1}{r^2}\frac{\partial}{\partial r}\left(r^2\frac{\partial}{\partial r}\right)\right] + \frac{\hat{L}^2}{2\mu r^2} + V(\mathbf{r})\right\}\langle\mathbf{r}|\hat{Q}|\phi_\alpha\rangle = \lambda_\alpha\langle\mathbf{r}|\hat{Q}|\phi_\alpha\rangle. \quad (31)$$

This can be solved with spherical Bessel functions $j_\ell(x)$ if we note the identity

$$x^2\frac{d^2}{dx^2}j_\ell(x) + 2x\frac{d}{dx}j_\ell(x) + [x^2 - \ell(\ell + 1)]j_\ell(x) = 0. \quad (32)$$

Let $x = k_{\ell,n}r$, where $k_{\ell,n} = \frac{\kappa_{\ell,n}}{a}$. Then, Eq. (32) takes the form

$$-\frac{1}{r^2}\frac{\partial}{\partial r}\left(r^2\frac{\partial}{\partial r}\right)j_\ell(k_{\ell,n}r) + \frac{\ell(\ell + 1)}{r^2}j_\ell(k_{\ell,n}) = k^2_{\ell,n}j_\ell(k_{\ell,n}). \quad (33)$$

Now substitute Eqs. (28) and (33) into Eq. (31) to get

$$\sum_{\ell=0}^{\infty}\sum_{m=-\ell}^{\ell}\sum_{n=1}^{\infty} C^\alpha_{\ell,m,n}N_{\ell,n}\left(\frac{\hbar^2k^2_{\ell,n}}{2\mu} + V(\mathbf{r})\right)j_\ell(k_{\ell,m}r)Y_\ell^m(\theta, \phi) = \lambda_\alpha\sum_{\ell=0}^{\infty}\sum_{m=-\ell}^{\ell}\sum_{n=1}^{\infty} C^\alpha_{\ell,m,n}N_{\ell,n}j_\ell(k_{\ell,m}r)Y_\ell^m(\theta, \phi). \quad (34)$$

If we multiply Eq. (34) by $j_{\ell_o}(k_{\ell_o,n_o}r)Y_{\ell_o,m_o}(\theta, \phi)$ and integrate over (r, θ, ϕ), we get

$$\frac{\hbar^2}{2m}\frac{\kappa^2_{\ell_o,n_o}}{a^2}C^\alpha_{\ell_o,m_o,n_o} + \sum_{\ell=0}^{\infty}\sum_{m=-\ell}^{\ell}\sum_{n=1}^{\infty}\langle\ell_o, m_o, n_o|V|\ell, m, n\rangle C^\alpha_{\ell,m,n} = \lambda_\alpha C^\alpha_{\ell_o,m_o,n_o}, \quad (35)$$

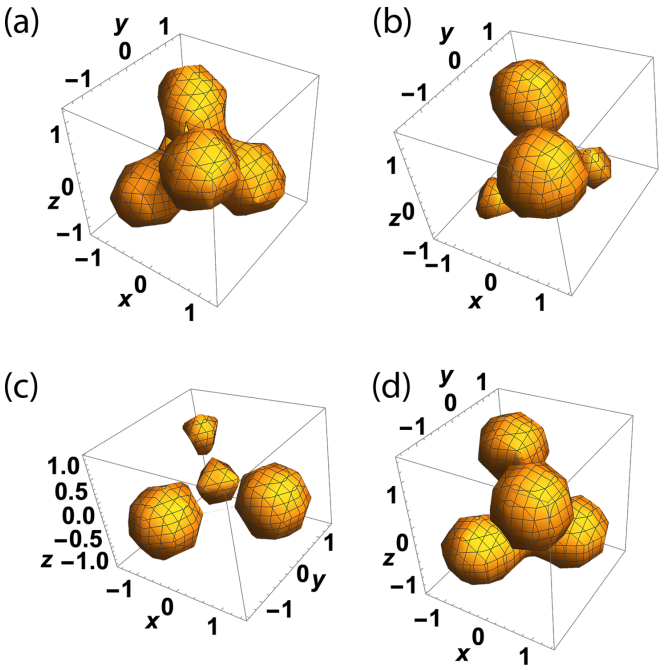

FIG. 3. Absolute value of the probability amplitude for bound states of the attractive tetrahedron. The bound states have energies (a) $E = -1.6837$ d.u., (b) $E = -0.48746$ d.u. (this state is antisymmetric about $y = 0$), (c) $E = -0.32975$ d.u. (this state is antisymmetric about $x = 0$), (d) $E = -0.30059$ d.u.

where

$$\langle \ell_o, m_o, n_o | V | \ell, m, n \rangle = N_{\ell_o,m_o,n_o} N_{\ell,m,n} \int_{\mathbf{R}} d\mathbf{r}\, j_{\ell_o}(k_{\ell_o,n_o} r) \times Y_{\ell_o,n_o}(\theta,\phi) V(\mathbf{r}) j_\ell(k_{\ell,n} r) Y_{\ell,m}(\theta,\phi). \quad (36)$$

We can solve Eq. (35) for the eigenvalues λ_α and coefficients $C^\alpha_{\ell_o,m_o,n_o}$, and then use the results to plot the eigenstates in the reaction region. For the attractive tetrahedron with $U_0 = -10$, there are four bound states which have energies $E = -1.6837$, $E = -0.48746$, $E = -0.32975$, and $E = -0.30059$. The absolute value of the probability amplitudes for the bound states (in Cartesian coordinates) is shown in Fig. 3 for the reaction region radius $a = 4$. The bound states sit in the potential wells of the tetrahedron. Although it is not shown explicitly in the figure, the bound state in Fig. 3(b) is antisymmetric about $y = 0$, and the bound state in Fig. 3(c) is antisymmetric about $x = 0$. There are no bound states for the repulsive tetrahedron.

B. Asymptotic region eigenstates

The Schrödinger equation for the asymptotic region can be written as

$$\langle \mathbf{r}|\hat{P}\hat{H}\hat{P}|E\rangle = \left\{ -\frac{\hbar^2}{2\mu}\left[\frac{1}{r^2}\frac{\partial}{\partial r}\left(r^2\frac{\partial}{\partial r}\right)\right] + \frac{\hat{L}^2}{2\mu r^2}\right\}\langle \mathbf{r}|\hat{P}|E\rangle = E\langle \mathbf{r}|\hat{P}|E\rangle, \quad (37)$$

and the basis states can be written as

$$\langle \mathbf{r}|\hat{P}|E\rangle = \sum_{\ell=0}^{\infty}\sum_{m=-\ell}^{\ell} \Phi_{\ell,m}(r) Y_{\ell,m}(\theta,\phi), \quad (38)$$

where

$$\Phi_{\ell,m}(r) = A_{\ell,m} h^{(2)}_\ell(kr) + B_{\ell,m} h^{(1)}_\ell(kr). \quad (39)$$

The spherical Hankel function $h^{(2)}_\ell(kr)$ denotes the incoming part of the wave function, and the spherical Hankel function $h^{(1)}_\ell(kr)$ denotes the outgoing part of the wave function.

C. The Wigner-Eisenbud *R* matrix

The first step to obtain an expression for the W-E R matrix is to consider again the projection of the eigenvalue equation (18) and note that the spectral decomposition of $\hat{Q}\hat{H}\hat{Q}$ is

$$\hat{Q}\hat{H}\hat{Q} = \sum_\alpha \lambda_\alpha \hat{Q}|\phi_\alpha\rangle\langle\phi_\alpha|\hat{Q}. \quad (40)$$

We can therefore write Eq. (18) in the form

$$\sum_\alpha \lambda_\alpha \hat{Q}|\phi_\alpha\rangle\langle\phi_\alpha|\hat{Q}|E\rangle + \hat{Q}\hat{H}\hat{P}|E\rangle = E\hat{Q}|E\rangle. \quad (41)$$

Now multiply by $\langle\phi_{\alpha'}|$, and use the orthonormality of the states $|\phi_\alpha\rangle$, to get so that

$$(\lambda_\alpha - E)\langle\phi_\alpha|\hat{Q}|E\rangle + \langle\phi_\alpha|\hat{Q}\hat{H}\hat{P}|E\rangle = 0. \quad (42)$$

The matrix element $\langle\phi_\alpha|\hat{Q}\hat{H}\hat{P}|E\rangle$ is computed in Appendix A.

Combining the result for $\langle\phi_\alpha|\hat{Q}\hat{H}\hat{P}|E\rangle$ obtained in Appendix A with Eq. (42), we can write

$$(\lambda_\alpha - E)\langle\phi_\alpha|\hat{Q}|E\rangle - \frac{\hbar^2 a^2}{2\mu}\sum_{\ell=0}^{\infty}\sum_{m=-\ell}^{\ell}\sum_{n=1}^{\infty} C^{\alpha *}_{\ell,m,n} N_{\ell,n} j_\ell(\kappa_{\ell,n}) \times \left(\frac{\partial \Phi_{\ell,m}(kr)}{\partial r}\right)_{r=a} = 0. \quad (43)$$

Now remember that

$$|E\rangle = \sum_{\alpha=1}^{\infty}\gamma_\alpha(E)\hat{Q}|\phi_\alpha\rangle + \Gamma_{\mathbf{k}}(E)\hat{P}|\Phi(\mathbf{k})\rangle, \quad (44)$$

so $\gamma_\alpha(E) = \langle\phi_\alpha|\hat{Q}|E\rangle$ and we finally obtain

$$(\lambda_\alpha - E)\gamma_\alpha(E) - \frac{\hbar^2 a^2}{2\mu}\sum_{\ell=0}^{\infty}\sum_{m=-\ell}^{\ell}\sum_{n=1}^{\infty}\xi^{\alpha *}_{\ell,m,n}(a) \times \left(\frac{\partial \Phi_{\ell,m}(kr)}{\partial r}\right)_{r=a} = 0, \quad (45)$$

where $\xi^{\alpha *}_{\ell,m,n}(r) = C^{\alpha *}_{\ell,m,n} N_{\ell,n} j_\ell(k_{\ell,n} r)$, so

$$\gamma_\alpha(E) = \frac{\hbar^2 a^2}{2\mu}\sum_{\ell=0}^{\infty}\sum_{m=-\ell}^{\ell}\sum_{n=1}^{\infty}\frac{\xi^{\alpha *}_{\ell,m,n}(a)}{(\lambda_\alpha - E)}\left(\frac{\partial \Phi_{\ell,m}(kr)}{\partial r}\right)_{r=a}. \quad (46)$$

Because the energy eigenstates can be divided into reaction region and asymptotic region contributions, we find that

$$\begin{aligned}\langle \mathbf{r}|E\rangle &= \sum_{\alpha=1}^{\infty}\gamma_\alpha(E)\langle \mathbf{r}|\hat{Q}|\phi_\alpha\rangle + \langle \mathbf{r}|\hat{P}|E\rangle \\ &= \sum_{\alpha=1}^{\infty}\gamma_\alpha(E)\sum_{\ell=0}^{\infty}\sum_{m=-\ell}^{\ell}\sum_{n=1}^{\infty}\xi^{\alpha}_{\ell,m,n}(r)Y_{\ell,m}(\theta,\phi) \\ &\quad + \sum_{\ell=0}^{\infty}\sum_{m=-\ell}^{\ell}\Phi_{\ell,m}(kr)Y_{\ell,m}(\theta,\phi). \end{aligned} \tag{47}$$

Next impose the condition that the scattering eigenstate $\langle r,\phi|E\rangle$ be continuous at $r=a$ so $\langle a,\phi|\hat{Q}|E\rangle = \langle a,\phi|\hat{P}|E\rangle$. This takes the form

$$\sum_{\alpha=1}^{\infty}\gamma_\alpha(E)\psi_{\alpha;\ell,m}(a) = \Phi_{\ell,m}(ka), \tag{48}$$

where $\psi_{\alpha;\ell,m}(a) = \sum_{n=1}^{\infty}\xi^{\alpha}_{\ell,m,n}(a) = \sum_{n=1}^{\infty}C^{\alpha}_{\ell,m,n}N_{\ell,n}j_\ell(\kappa_{\ell,n})$. Combining Eqs. (46) and (48), we obtain

$$\begin{aligned}&\frac{\hbar^2a^2}{2\mu}\sum_{\ell'=0}^{\infty}\sum_{m'=-\ell'}^{\ell'}\frac{\psi_{\alpha;\ell,m}(a)\psi^*_{\alpha;\ell',m'}(a)}{(\lambda_\alpha - E)}\left(\frac{\partial\Phi_{\ell',m'}(kr)}{\partial r}\right)_{r=a} \\ &\quad = \Phi_{\ell,m}(ka). \end{aligned} \tag{49}$$

The R matrix is obtained from the condition

$$\sum_{\ell'=0}^{\infty}\sum_{m'=-\ell'}^{\ell'}aR_{\ell,m;\ell',m'}(E)\left(\frac{\partial\Phi_{\ell',m'}(kr)}{\partial r}\right)_{r=a} = \Phi_{\ell,m}(ka). \tag{50}$$

Therefore, the R matrix is given by

$$R_{\ell,m;\ell',m'}(E) = \frac{\hbar^2a}{2\mu}\sum_{\alpha=1}^{\infty}\frac{\psi_{\alpha;\ell,m}(a)\psi^*_{\alpha;\ell',m'}(a)}{(\lambda_\alpha - E)}. \tag{51}$$

If we substitute this expression for the W-E R matrix into Eq. (14), we obtain an explicit expression for the scattering matrix for the tetrahedral system. Below we show the results of this scattering theory for both an attractive tetrahedron and a repulsive tetrahedron.

V. SCATTERING FROM AN ATTRACTIVE TETRAHEDRON

We used the W-E theory described above to compute the scattering matrix for the eigenstate basis $\ell = 0,\ldots,7$; $-\ell \leqslant m \leqslant \ell$; $n = 1,\ldots,8$. The radial quantum numbers n are summed over when computing the R matrix. For this basis, the S matrix is then a 512×512 matrix composed of scattering amplitudes for all possible scattering processes $\{\ell_1,m_1\}\rightarrow\{\ell_2,m_2\}$ for $\ell = 0,\ldots,7$; $-\ell\leqslant m\leqslant\ell$. The scattering matrix elements are labeled left to right and top to bottom in the order

$$\begin{aligned}\{\ell,m\} = \{&(0,0),(1,-1),(1,0),(1,+1),\\ &\times(2,-2),(2,-1),\ldots,(2,+2),(3,-3),\ldots.\end{aligned}$$

In Fig. 4, we show the absolute value of four S-matrix elements as a function of energy. Figure 4(a) shows $|S_{3,3}|$ as a function of energy. $|S_{3,3}|$ is the square root of the probability for an incoming particle with angular momentum $\{\ell=1,m=0\}$ to scatter as an outgoing particle with angular momentum $\{\ell=1,m=0\}$. Note that there are scattering resonances in the neighborhoods of energies $E=0.6$, $E=2.8$, $E=3.8$, and $E=6$. Figure 4(b) shows $|S_{5,3}|$ as a function of energy. $|S_{5,3}|$ is the square root of the probability to scatter from $\{\ell=2,m=-2\}$ to $\{\ell=1,m=0\}$. Figure 4(c) shows $|S_{6,4}|$ as a function of energy. $|S_{6,4}|$ is the square root of the probability to scatter from $\{\ell=2,m=-1\}$ to $\{\ell=1,m=+1\}$. Figure 4(d) shows $|S_{9,5}|$ as a function of energy. $|S_{9,5}|$ is the square root of the probability to scatter from $\{\ell=2,m=+2\}$ to $\{\ell=2,m=-2\}$. All four scattering processes have scattering resonances in the neighborhood of energies $E=0.6$, $E=2.8$, $E=3.8$, and $E=6$.

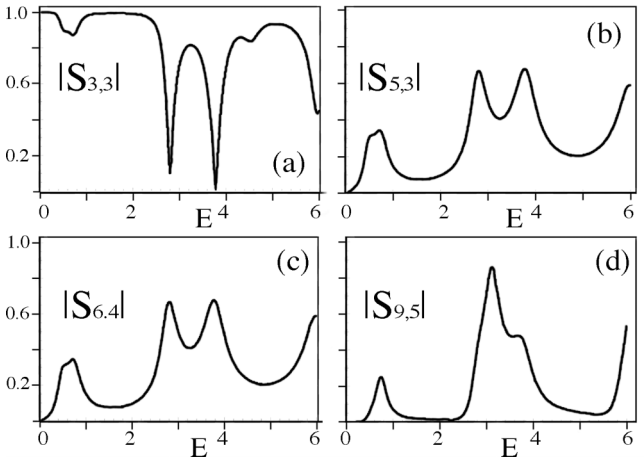

FIG. 4. Absolute value of scattering amplitude for $U_0=-10$ and incident energy $E=0\rightarrow6$ d.u. (a) $|S_{3,3}|$ scattering amplitude for $\{\ell,m\}=\{1,0\}\rightarrow\{1,0\}$. (b) $|S_{5,3}|$ scattering amplitude for $\{\ell,m\}=\{2,-2\}\rightarrow\{1,0\}$. (c) $|S_{6,4}|$ scattering amplitude for $\{\ell,m\}=\{2,-1\}\rightarrow\{1,+1\}$. (d) $|S_{9,5}|$ scattering amplitude for $\{\ell,m\}=\{2,+2\}\rightarrow\{2,-2\}$. Peaks and dips are due to quasibound-state scattering resonances.

In Fig. 5, we plot the absolute value of S-matrix elements S_{n_1,n_2} with $n_1=1,\ldots,16$ and $n_2=1,\ldots,16$. This corresponds to scattering amplitudes between all angular-momentum states $\ell=0,\ldots,3$ and the corresponding values of m. In these plots, we only show values of $|S_{n_1,n_2}|>0.2$ so that we pick up the dominant scattering processes. In Figs. 5(a), 5(c), and 5(d), we show the S matrix for energies $E=0.435$, $E=2.76$, and $E=3.8$, which are energies at which scattering resonances occur in Fig. 4. At these energies, there are multiple transitions between different angular momenta. In Fig. 5(b), we show the S matrix for energy $E=1.5$ which is an energy at which no significant scattering occurs in Fig. 4.

In Fig. 6, we show the poles of the S-matrix element $S_{3,3}$ in the complex energy plane. All of the scattering resonances that appear in Fig. 4 can be associated with poles of the S matrix in the complex energy plane. Note that the imaginary part of the energy increases as the real part of the energy increases. This indicates that the higher energy quasibound states have shorter lifetime than the lower-energy quasibound states because the lifetime is proportional to $\hbar/\mathrm{Im}(E)$ (in dimensioned units).

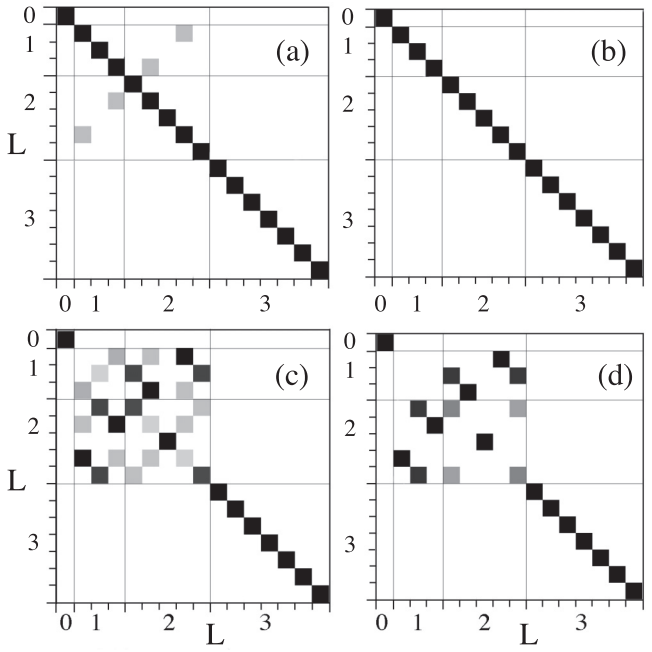

FIG. 5. Plots of the absolute value of S-matrix elements for attractive potential $U_0 = -10$ d.u.: (a) at resonance $E = 0.435$ d.u., (b) off resonance $E = 1.5$ d.u., (c) at resonance $E = 2.76$ d.u., (d) at resonance $E = 3.8$ d.u. Only matrix elements with absolute value greater than 0.2 are plotted.

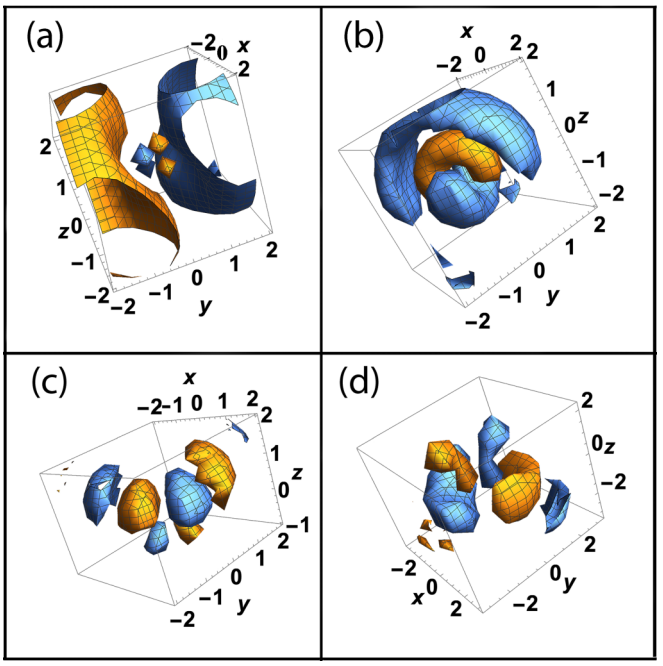

FIG. 7. Quasibound states of the attractive tetrahedron with energies (a) $E = +0.43186$ d.u., (b) $E = 2.65181$ d.u., (c) $E = 2.75598$ d.u., (d) $E = 3.8135$ d.u. These are *localized* reaction region states.

Finally, in Fig. 7, we show some of the quasibound states (reaction region eigenstates) that give rise to the scattering resonances. All the states in Fig. 7 sit in, or are tightly wrapped around, the position of the potential wells of the tetrahedron. The state in Fig. 7(a), with energy $E = +0.43186$ is purely imaginary. The lighter (orange) surface in Fig. 7(a) has the value $\mathrm{Im}[\phi_6(\mathbf{r})] = -0.06034$ and the darker (blue) surface has the value $\mathrm{Im}[\phi_6(\mathbf{r})] = +0.06034$. The state in Fig. 7(b), with energy $E = +2.65181$, is real. The lighter (orange) surface in Fig. 7(b) has the value $\mathrm{Re}[\phi_{30}(\mathbf{r})] = -0.08861$, and the darker (blue) surface has value $\mathrm{Re}[\phi_{30}(\mathbf{r})] = +0.04315$. The state in Fig. 7(c), with energy $E = +2.75598$, is purely imaginary. The lighter (orange) surface in Fig. 7(c) has he value $\mathrm{Im}[\phi_{31}(\mathbf{r})] = -0.07974$, and the darker (blue) surface has the value $\mathrm{Im}[\phi_{31}(\mathbf{r})] = +0.07974$. The state in Fig. 7(d), with energy $E = +3.8135$, is purely imaginary. The lighter (orange) surface has the value $\mathrm{Im}[\phi_{48}(\mathbf{r})] = -0.09246$, and the darker (blue) surface has value $\mathrm{Im}[\phi_{48}(\mathbf{r})] = +0.09246$. In the neighborhood of each of the energies listed, there are several quasibound states. We have only shown a selected few quasibound states here. Each of these states can be associated with the poles of the S matrix shown in Fig. 6.

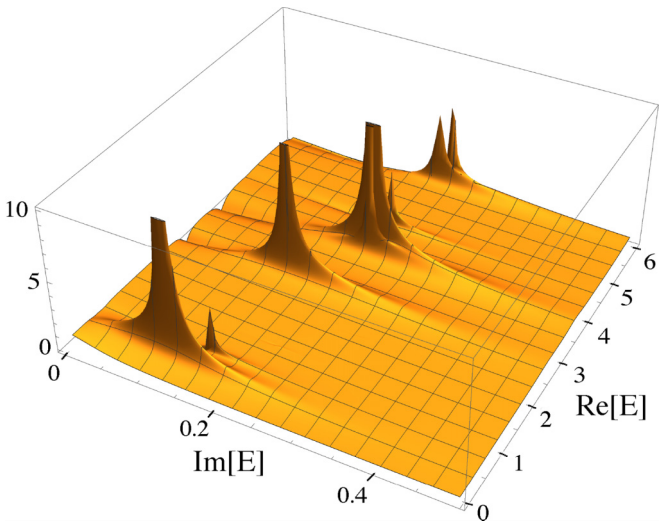

FIG. 6. S-matrix poles obtained from $S_{3,3}$ for the attractive potential.

As pointed out in Ref. [29], for scattering systems without a well-defined boundary, such as the tetrahedral system we are considering here, the reaction region contains two types of states: *localized states*, whose probability distribution is localized in the neighborhood of the potential energy and do not depend on the size of the reaction region; and *extended states*, which only see the walls of the reaction region and are not influenced by the potential energy. In Fig. 8, we show some examples of extended reaction region states. The state in Fig. 8(a), with energy $E = +1.27137$, is real. The lighter (orange) surface in Fig. 8(a) has value $\mathrm{Im}[\phi_{15}(\mathbf{r})] = -0.08872$, and the darker (blue) surface has value $\mathrm{Im}[\phi_{15}(\mathbf{r})] = +0.08601$. The state in Fig. 8(b), with energy $E = +1.99251$, is real. The lighter (orange) surface in Fig. 8(b) has the value $\mathrm{Re}[\phi_{28}(\mathbf{r})] = -0.08911$, and the darker (blue) surface has the value $\mathrm{Re}[\phi_{28}(\mathbf{r})] = +0.09789$. The state in Fig. 8(c), with energy $E = +2.75598$, is purely imaginary. The lighter (orange) surface in Fig. 7(c) has value $\mathrm{Im}[\phi_{36}(\mathbf{r})] = -0.1353$, and the darker (blue) surface has the value $\mathrm{Im}[\phi_{36}(\mathbf{r})] = +0.1353$. The state in Fig. 8(d), with

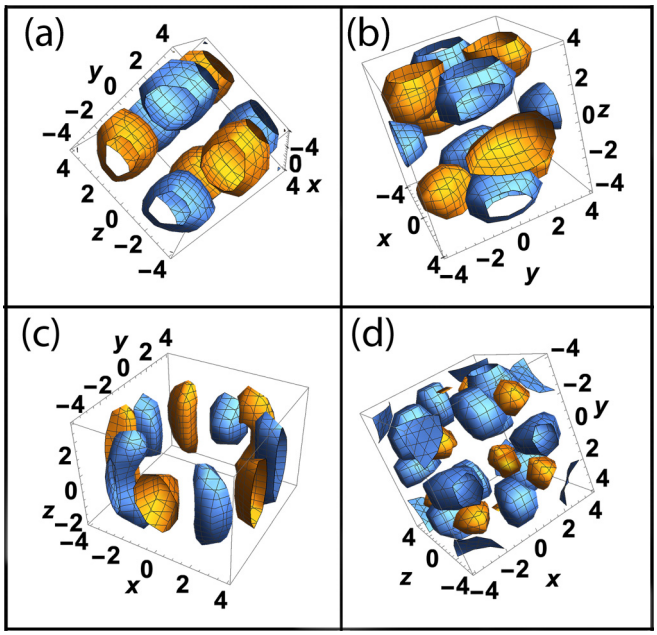

FIG. 8. *Extended* reaction region states of the attractive tetrahedron with energies (a) $E = +1.27137$ d.u., (b) $E = +1.99251$ d.u., (c) $E = +2.85299$ d.u., (d) $E = +3.8524$ d.u.

energy $E = +3.8524$ is real. The lighter (orange) surface in Fig. 8(d) has value $\mathrm{Re}[\phi_{48}(\mathbf{r})] = -0.1470$, and the darker (blue) surface has the value $\mathrm{Re}[\phi_{48}(\mathbf{r})] = +0.0629$.

VI. SCATTERING FROM A REPULSIVE TETRAHEDRON

To obtain the repulsive tetrahedral potential, we set $U_0 = +10$. The repulsive tetrahedron has no bound states, but it does have quasibound states. Evidence for this comes from scattering resonances and poles of the S matrix in the complex energy plane.

In Fig. 9, we show four S-matrix elements as a function of energy. Figure 4(a) shows that $|S_{3,3}|$ is the square root of the probability for an incoming particle with angular momentum $\{\ell = 1, m = 0\}$ to scatter as an outgoing particle with angular momentum, $\{\ell = 1, m = 0\}$. Note that there are weak scattering resonances in the neighborhoods of energies $E = 2.6$, $E = 3.6$, and $E = 6$. Figure 4(b) shows $|S_{5,3}|$ as a function of energy. $|S_{5,3}|$ is the square root of the probability to scatter from $\{\ell = 2, m = -2\}$ to $\{\ell = 1, m = 0\}$. Figure 4(c) shows $|S_{6,4}|$ as a function of energy. $|S_{6,4}|$ is the square root of the probability to scatter from $\{\ell = 2, m = -1\}$ to $\{\ell = 1, m = +1\}$. Figure 4(d) shows $|S_{9,5}|$ as a function of energy. $|S_{9,5}|$ is the square root of the probability to scatter from $\{\ell = 2, m = +2\}$ to $\{\ell = 2, m = -2\}$. All four scattering processes have scattering resonances in the neighborhood of energies $E = 2.6$, $E = 3.6$, and $E = 6$.

In Fig. 10, we plot the absolute value of S-matrix elements S_{n_1,n_2} with $n_1 = 1, \ldots, 16$ and $n_2 = 1, \ldots, 16$. This corresponds to scattering amplitudes between all angular-momentum states $\ell = 0, \ldots, 3$ and the corresponding values of m. In these plots, we only show values of $|S_{n_1,n_2}| > 0.1$ so that we pick up the dominant scattering processes. In Fig. 10(a), we show the S matrix for energy $E = 0.7$ which is

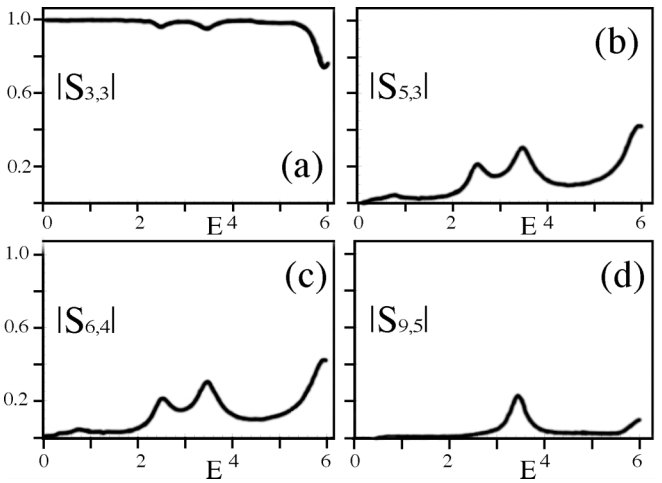

FIG. 9. Absolute value of scattering amplitude for $U_0 = +10$ and incident energy $E = 0 \rightarrow 6$ d.u. (a) $|S_{3,3}|$ scattering amplitude for $\{\ell, m\} = \{1, 0\} \rightarrow \{1, 0\}$. (b) $|S_{5,3}|$ scattering amplitude for $\{\ell, m\} = \{2, -2\} \rightarrow \{1, 0\}$. (c) $|S_{6,4}|$ scattering amplitude for $\{\ell, m\} = \{2, -1\} \rightarrow \{1, +1\}$. (d) $|S_{9,5}|$ scattering amplitude for $\{\ell, m\} = \{2, +2\} \rightarrow \{2, -2\}$. Peaks and dips are due to quasibound-state scattering resonances.

an energy at which no significant scattering occurs in Fig. 9. In Figs. 10(b)–10(d), we show the S matrix for energies $E = 2.5$, $E = 3.5$, and $E = 5.9$, which are energies at which scattering resonances occur in Fig. 9. At these energies there are multiple transitions between different angular momenta.

In Fig. 11, we show the poles of the S-matrix element $S_{3,3}$ in the complex energy plane. The scattering resonances

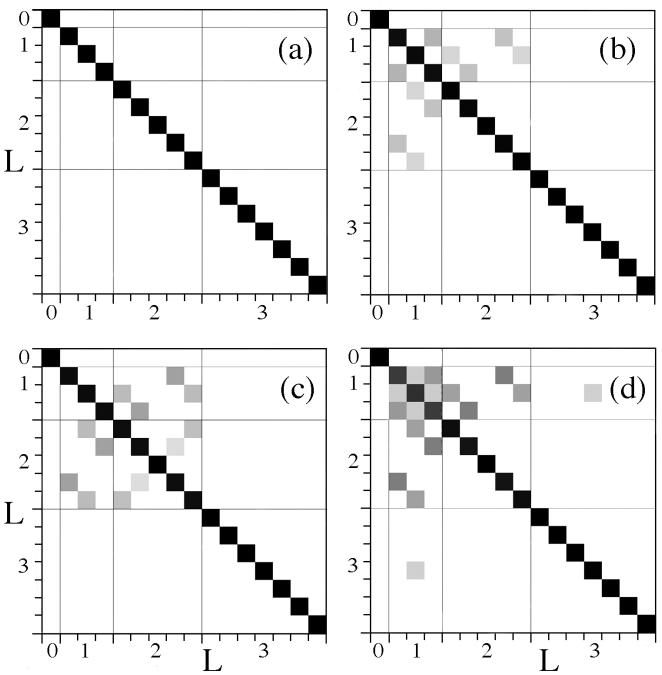

FIG. 10. Plots of the absolute value of S-matrix elements for $U_0 = +10$ d.u.: (a) at apparent resonance $E = 0.70$ d.u., (b) at resonance $E = 2.5$ d.u., (c) at resonance $E = 3.5$ d.u., (d) at resonance $E = 5.9$ d.u. Only matrix elements with absolute value greater than 0.1 are plotted.

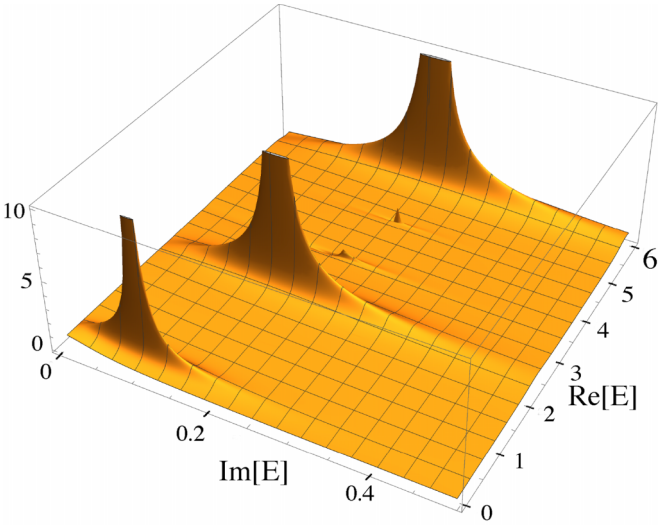

FIG. 11. S-matrix poles for $S_{3,3}$ for the repulsive potential.

that appear in Fig. 4 can be associated with poles of the S matrix in the complex energy plane. Note that the complex part of the energy increases as the real part of the energy increases, indicating that the higher-energy quasibound states have shorter lifetime than the lower-energy quasibound states.

Finally in Fig. 12, we show some of the quasibound states (localized reaction region eigenstates) that give rise to the scattering resonances for the repulsive tetrahedron. All the states in Fig. 12 sit in the neighborhood of the potential peaks of the tetrahedron. The state in Fig. 12(a), with energy $E = +2.47325$, is real. The lighter (orange) surface in Fig. 12(a) has the value $\mathrm{Re}[\phi_{28}(\mathbf{r})] = -0.06773$, and the darker (blue) surface has the value $\mathrm{Re}[\phi_{28}(\mathbf{r})] = +0.07162$. The state in Fig. 12(b), with energy $E = +2.51459$ is purely imaginary. The lighter (orange) surface in Fig. 12(b) has the value $\mathrm{Im}[\phi_{29}(\mathbf{r})] = -0.07256$, and the darker (blue) surface has the value $\mathrm{Im}[\phi_{29}(\mathbf{r})] = +0.07256$. The state in Fig. 12(c), with energy $E = +3.42772$ is real. The lighter (orange) surface in Fig. 12(c) has value $\mathrm{Re}[\phi_{42}(\mathbf{r})] = -0.05065$, and the darker (blue) surface has the value $\mathrm{Re}[\phi_{42}(\mathbf{r})] = +0.09413$. The state in Fig. 12(d), with energy $E = +3.47192$, is purely imaginary. The lighter (orange) surface in Fig. 12(d) has the value $\mathrm{Im}[\phi_{43}(\mathbf{r})] = -0.08618$, and the darker (blue) surface has the value $\mathrm{Im}[\phi_{43}(\mathbf{r})] = +0.08618$. In the neighborhood of each of the energies listed, there are several quasibound states. We have only shown a selected few quasibound states here. Each one of these states can be associated with the poles of the S matrix shown in Fig. 11.

The repulsive tetrahedron also has a series of extended reaction region states which look very much like those shown in Fig. 8.

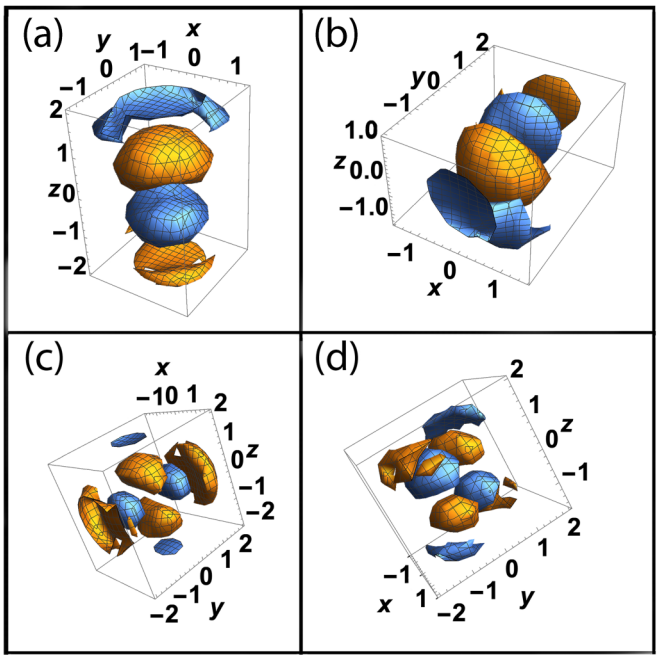

FIG. 12. Quasibound states of the repulsive tetrahedron with energies (a) $E = 2.47325$ d.u., (b) $E = 2.51459$ d.u., (c) $E = 3.42772$ d.u., (d) $E = 3.47192$ d.u. These are localized states of the reaction region.

VII. CONCLUSIONS

Wigner-Eisenbud scattering theory provides an efficient method to visualize quasibound-state structures in the neighborhood of small quantum objects, such as small molecules. Quasibound states are unstable standing waves associated with parts of the molecule that can dissociate from the main structure. Because they are unstable, they are difficult to visualize.

For a simple molecule-size tetrahedral quantum structure, we have found that quasibound electron states can exist in the positive-energy continuum when the tetrahedron is composed either of four attractive potential wells or four repulsive potential wells. It is well known that W-E theory provides an efficient means to model the scattering dynamics of small quantum objects but, as we have shown above, it also provides an efficient means to visualize the spatial structure of three-dimensional unstable standing-wave structures.

ACKNOWLEDGMENTS

The authors thank the Robert A. Welch Foundation (Grant No. F-1051) for support of this work.

APPENDIX

We can obtain an explicit form for the matrix element $\hat{Q}\hat{H}\hat{P}$:

$$\hat{Q}\hat{H}\hat{P} = -\hat{Q}\hat{V}\hat{P} = \frac{2\hbar^2}{\mu a^2}\oint_{\mathbf{R}} d\mathbf{r}_1 \oint_{\mathbf{A}} d\mathbf{r}_2 |\mathbf{r}_1\rangle\langle\mathbf{r}_1|\mathbf{r}_2\rangle\delta(r_2 - a)\frac{\partial}{\partial r_2}\langle\mathbf{r}_2|. \tag{A1}$$

This then takes the form

$$\begin{aligned}\langle\phi_\alpha|\hat{Q}\hat{H}\hat{P}|E\rangle &= -\frac{2\hbar^2}{\mu a^2}\int_0^a r_1^2 dr_1\int_a^\infty r_2^2 dr_2\int d\Omega_1\delta(r_1-r_2)\delta(r_2-a)\langle\phi_\alpha|r_1,\theta_1,\phi_1\rangle\frac{\partial}{\partial r_2}\langle r_2,\theta_1,\phi_1|\hat{P}|E\rangle\\ &= -\frac{2\hbar^2}{\mu a^2}\int_0^a r_1^2 dr_1\int_a^\infty r_2^2 dr_2\int d\Omega_1\delta(r_1-r_2)\delta(r_2-a)\sum_{\ell'=0}^{\infty}\sum_{m'=-\ell'}^{\ell'}\sum_{n'=1}^{\infty}C^{\alpha*}_{\ell',m',n'}N_{\ell',n'}j_{\ell'}(k_{\ell',n'}r_1)Y_{\ell',m'}(\theta_1,\phi_1)\\ &\quad\times\frac{\partial}{\partial r_2}\left(\sum_{\ell=0}^{\infty}\sum_{m=-\ell}^{\ell}\Phi_{\ell,m}(kr_2)Y_{\ell,m}(\theta_1,\phi_1)\right),\end{aligned}\tag{A2}$$

where $d\Omega_1 = \sin(\theta_1)d\theta_1 d\phi_1$.

Integrate over θ_1 and ϕ_1 and sum over ℓ' and m' to get

$$\langle\phi_\alpha|\hat{Q}\hat{H}\hat{P}|E\rangle = -\frac{2\hbar^2}{\mu a^2}\int_0^a r_1^2 dr_1\int_a^\infty r_2^2 dr_2\delta(r_1-r_2)\delta(r_2-a)\sum_{\ell=0}^{\infty}\sum_{m=-\ell}^{\ell}\sum_{n'=1}^{\infty}C^{\alpha*}_{\ell,m,n'}N_{\ell,n'}j_\ell(k_{\ell,n'}r)\frac{\partial}{\partial r_2}[\Phi_{\ell,m}(kr_2)].\tag{A3}$$

Note that since δ functions are even functions with area equal to one, when they are evaluated at the limits of integration $r = a$, only one half of the δ function contributes and they each give a factor of $\frac{1}{2}$. We obtain

$$\langle\phi_\alpha|\hat{Q}\hat{H}\hat{P}|E\rangle = -\frac{\hbar^2 a^2}{2\mu}\sum_{\ell=0}^{\infty}\sum_{m=-\ell}^{\ell}\sum_{n=1}^{\infty}C^{\alpha*}_{\ell,m,n}N_{\ell,n}j_\ell(\kappa_{\ell,n})\left(\frac{\partial\Phi_{\ell,m}(kr)}{\partial r}\right)_{r=a}.\tag{A4}$$

[1] R. D. Levine, Acc. Chem. Res. **3**, 273 (1970).
[2] A. Bergeat, J. Onvlee, C. Naulin, A. van der Avoird, and M. Costes, Nat. Chem. **7**, 349 (2015).
[3] S. Cohen, M. M. Harb, A. Ollagnier, F. Robicheaux, M. J. J. Vrakking, T. Barillot, F. Lepine, and C. Bordas, Phys. Rev. Lett. **110**, 183001 (2013).
[4] S. Cohen, M. M. Harb, A. Ollagnier, F. Robicheaux, M. J. J. Vrakking, T. Barillot, F. Lepine, and C. Bordas, Phys. Rev. A **94**, 013414 (2016).
[5] A. M. Barr and L. E. Reichl, Phys. Rev. A **81**, 022707 (2010).
[6] E. P. Wigner and L. E. Eisenbud, Phys. Rev. **72**, 29 (1947).
[7] A. M. Lane and R. G. Thomas, Rev. Mod. Phys. **30**, 257 (1958).
[8] D. Baye, Phys. Rep. **565**, 1 (2015).
[9] H. A. Weidenmuller, Ann. Phys. (NY) **158**, 120 (1984).
[10] J. J. M. Verbaarschot, H. A. Weidenmuller, and M. R. Zirnbauer, Phys. Rep. **129**, 367 (1985).
[11] P. G. Burke and W. D. Robb, Adv. At. Mol. Phys. **11**, 143 (1975).
[12] R. K. Nesbet, *Variational Methods in Electron-Atom Scattering Theory* (Plenum Press, New York, 1980).
[13] M. Aymer, C. H. Greene, and E. Luc-Koenig, Rev. Mod. Phys. **68**, 1015 (1996).
[14] O. Zatsarinny and K. Bartschat, J. Phys. B: At. Mol. Opt. Phys. **46**, 112001 (2013).
[15] J. D. Gorfinkiel, L. A. Morgan, and J. Tennyson, J. Phys. B: At. Mol. Opt. Phys. **35**, 543 (2002).
[16] S. Tonzani and C. H. Greene, J. Chem. Phys. **124**, 054312 (2006).
[17] D. Bouchiha, J. D. Gorfinkiel, L. G. Caron, and L. Sanche, J. Phys. B: At. Mol. Opt. Phys. **39**, 975 (2006).
[18] N. Douguet, V. Kokoouline, and A. E. Orel, J. Phys. B: At. Mol. Opt. Phys. **45**, 051001 (2012).
[19] A. M. Barr, K. Na, and L. E. Reichl, Phys. Rev. A **83**, 062510 (2011).
[20] A. Barr and L. E. Reichl, Fortschr. Phys. **61**, 59 (2013).
[21] G. Akguc and L. E. Reichl, Phys. Rev. E **64**, 056221 (2001); **67**, 046202 (2003).
[22] H. Lee and L. E. Reichl, Phys. Rev. B **77**, 205318 (2008); **79**, 193305 (2009)
[23] H. Lee and L. E. Reichl, J. Phys. A: Math. Theor. **43**, 405303 (2010).
[24] L. E. Reichl and M. D. Porter, Phys. Rev. E **97**, 042206 (2018).
[25] B. Eckhardt, J. Phys. A: Math. Gen. **20**, 5971 (1987).
[26] P. Gaspard and S. A. Rice, J. Chem. Phys. **90**, 2225 (1989); **90**, 2242 (1989); **90**, 2255 (1989).
[27] M. D. Porter, A. Barr, A. Barr, and L. E. Reichl, Phys. Rev. E **95**, 052213 (2017).
[28] A. Barr, A. Barr, M. D. Porter, and L. E. Reichl, Chaos **27**, 104604 (2017).
[29] M. D. Porter, A. Barr, A. Barr, and L. E. Reichl, Physica B (Amsterdam, Neth.) **571**, 162 (2019).
[30] Q. H. Song, L. Ge, A. D. Stone, H. Cao, J. Wiersig, J.-B. Shim, J. Unterhinninghofen, W. Fang, and G. S. Soloman, Phys. Rev. Lett. **105**, 103902 (2010).
[31] J. U. Nöckel and A. D. Stone, Nature (London) **385**, 45 (1997).
[32] B. Redding, A. Cerjan, X. Huang, M. L. Lee, A. D. Stone, M. A. Choma, and H. Cao, Proc. Natl. Acad. Sci. USA **112**, 1304 (2015).
[33] S. Ree and L. E. Reichl, Phys. Rev. E **60**, 1607 (1999).
[34] J. Dudek, A. Gozdz, N. Schunck, and M. Miskiewicz, Phys. Rev. Lett. **88**, 252502 (2002).
[35] J. Dudek, D. Curien, N. Dubray, J. Dobaczewski, V. Pangon, P. Olbratowski, and N. Schunck, Phys. Rev. Lett. **97**, 072501 (2006).
[36] J. Dudek, D. Curien, I. Dedes, K. Mazurek, S. Tagami, Y. R. Shimizu, and T. Bhattacharjee, Phys. Rev. C **97**, 021302(R) (2018).

[37] P. J. Stewart, Found. Chem. **20**, 111 (2018).
[38] D. Sweet, E. Ott, and J. A. Yorke, Nature (London) **399**, 315 (1999).
[39] S. M. Reimann, M. Koskinen, H. Häkkinen, P. E. Lindelof, and M. Manninen, Phys. Rev. B **56**, 12147 (1997).
[40] C. Bloch, Nucl. Phys. **4**, 503 (1957).
[41] H. Feshbach, Ann. Phys. (NY) **19**, 287 (1962).
[42] J. D. Head, K. A. R. Mitchell, L. Noodleman, and N. L. Paddock, Can. J. Chem. **55**, 669 (1977).